RSC Advances

PAPER

View Article Online
View Journal | View Issue

Check for updates

Cite this: *RSC Adv.*, 2023, **13**, 13423

Synthesis, photoluminescence, Judd–Ofelt analysis, and thermal stability studies of Dy^{3+}-doped $BaLa_2ZnO_5$ phosphors for solid-state lighting applications

Irfan Ayoub [ab] and Vijay Kumar *[ab]

Here, we report a series of white-emitting $Ba(La_{2-x}Dy_x)ZnO_5$ (x = 0–7 mol%) phosphors synthesized *via* a high-temperature solid-state reaction. The synthesized phosphor's phase purity and tetragonal crystal structure were confirmed by an X-ray powder diffraction (XRPD) pattern. The wide bandgap characteristic feature was assessed through reflectance spectra, and the estimated bandgap was found to be 4.70 eV. Besides analyzing the effect of doping on the surface morphology, the distribution of ions on the surface was observed through the secondary ion mass spectroscopy technique. The synthesized phosphor was found to display bluish (486 nm) and yellowish (576 nm) bands in the emission spectra under the excitation of 325 nm and 352 nm, which together are responsible for producing the white luminescence. The analysis of Judd–Ofelt parameters indicates the symmetric nature of Dy^{3+} substitution in the present host. The thermal stability of the phosphor was assessed by varying the temperature up to 403 K, and it was found that the synthesized phosphor possesses improved thermal stability with an activation energy of 0.29 eV. The photometric evaluations of the present phosphor revealed the CIE coordinates around the near-white regime (0.3448, 0.3836), along with the color-correlated temperature value of 5102 K. All research on this luminescent material's unique features points to the possibility of using it to fabricate white-light-emitting devices for solid-state lighting applications.

Received 21st April 2023
Accepted 26th April 2023

DOI: 10.1039/d3ra02659k

rsc.li/rsc-advances

Open Access Article. Published on 03 2023. Downloaded on 2025/5/31 23:29:15.
This article is licensed under a Creative Commons Attribution-NonCommercial 3.0 Unported Licence.

Introduction

The digital world of today is experiencing a considerable energy shortage due to the development of technology and the inefficient use of the world's energy resources, particularly for lighting.[1] If available energy is not used cautiously and properly, catastrophic scenarios will occur sooner rather than later. Thus, it is crucial to encourage and simultaneously look for effective energy-saving measures to avoid these disastrous scenarios.[2] After considering the causes, it appears that the key factor is the inefficiency displayed by machinery that consume a huge amount of energy but generate very little in return. The key to lowering energy usage in this area is carefully selecting high-efficiency phosphors because light is crucial to our everyday lives in the twenty-first century.[3] Phosphors are light-emitting materials composed of a host matrix and an activator.[4] These materials possess the capability to transform light from its higher frequency domain to a lower frequency domain *via* different electronic transitions.[5] Phosphor materials are regarded as an affordable energy source that can satisfy present and future energy demands on a worldwide basis. According to a recent report by the US Department of Energy, LEDs are expected to reduce lighting energy consumption by 15% in 2020 and by 40% in 2030, saving 3.0 quads in 2030 alone, which would amount to over $26 billion in savings at the current price of energy.[6,7] Additionally, these energy savings would result in a 180 million metric ton reduction in greenhouse gas emissions. During the next ten years, the DOE predicts that the traditional methods of illuminating our planet, which began with incandescent light bulbs and progressed to overhead fluorescent ones, may become outdated.[8]

Several fields of science and technology have undergone a tremendous transformation because of phosphor-based lighting technology.[9] For application in solid-state lighting systems, researchers are continuously studying various phosphor materials that are reliable, inexpensive, eco-friendly, have a longer lifespan, *etc.*[10,11] At the moment, multidisciplinary efforts are being made with an emphasis on creating phosphor materials with improved luminous properties.[2] In several inorganic host matrices, rare-earth (RE) ions are known to be effective initiators for luminous centers. They are extremely

[a]*Department of Physics, National Institute of Technology Srinagar, Jammu and Kashmir – 190006, India. E-mail: vj.physics@gmail.com*
[b]*Department of Physics, University of the Free State, P.O. Box 339, Bloemfontein ZA9300, South Africa*

© 2023 The Author(s). Published by the Royal Society of Chemistry

Open Access Article. Published on 03 2023. Downloaded on 2025/5/31 23:29:15.
This article is licensed under a Creative Commons Attribution-NonCommercial 3.0 Unported Licence.

effective in increasing the quantum efficiency of phosphors because of their special electronic structures, which consist of partially filled 4f shells surrounded by $5s^2$ and $5p^6$ electrons.[12,13] Controlling the optical and photoluminescence (PL) properties of various host matrixes is possible by using the RE ions as an dopants.[13] Nonetheless, the research community has focused on creating white-light-emitting diodes (wLEDs) with efficient characteristic parameters and efficiency since they may be used effectively for lighting and many display applications.[14] At the beginning of phosphor technology, wLEDs were developed by combining UV/blue LEDs with appropriate phosphor material. However, these wLEDs were found to have inappropriate CRI and CCT values due to a lack of red components in the emission spectra.[15,16] Later on, wLEDs were developed by coating the near-UV LED chips with tricolor (red, green, and blue) phosphor materials. But it was found that wLEDs developed *via* this process possess a very short lifetime and lack the features of eco-friendliness due to the presence of a poor red component.[3] Continuing with the aim of fabricating efficient wLEDs, researchers have developed an interest in fabricating single-composition wLED phosphor materials.[1,17] In this regard, trivalent dysprosium (Dy^{3+}) is thought to be an efficient activator for the fabrication of wLEDs due to its strong white emission. Dy^{3+}-ion possesses a complex intra-4f electronic configurational band that allows a wide range of electronic transitions, thereby exhibiting better white emission spectra composed of yellow (Y) and bluish (B) bands when excited by near UV wavelengths. Thus, the optimization of the bands (Y and B) results in the generation of effective white light.[18,19]

For the generation of white light, different varieties of host matrices have been explored, such as phosphates, oxides, sulfates, aluminates, vanadates, *etc.*[20–26] Amongst all the mentioned host matrices, oxide hosts are considered to be the most important because of their characteristic features like stable crystal structure, ease of synthesis, economical, increased tensile strength, high chemical and thermal stability, moisture resistance, and most importantly, their eco-friendly nature.[20,27,28] Furthermore, the oxide host materials were found to have a broad bandgap and inefficient luminous characteristics. Among the different oxide hosts, $BaLa_2ZnO_5$ is considered an efficient luminous host due to its stable crystal structure and thermal stability.[29] The structural framework of this host is comprised of ten- and eight-fold polyhedra of BaO_{10} and LaO_8, with C_{2v} and D_4 symmetry, respectively, and four-fold coordinate sites occupied by Zn^{2+}.[30] In light of the above discussion, $BaLa_2ZnO_5$ was selected for the presented study as it is an enigmatic host for different structural and optical studies.

There have been several past articles on this host, such as Song *et al.*,[31] studied the thermometric properties of Bi^{3+}/Sm^{3+}-doped $BaLa_2ZnO_5$. Using the combustion approach, Sehrawat *et al.*[30,32] investigated the green and white light emissions caused by the emissions of Er^{3+} and Dy^{3+} doping in the host. The sol–gel approach was used by Singh *et al.*[33,34] for studying the luminescence properties of Sm^{3+} and Tb^{3+} doping in $BaLa_2ZnO_5$. Using the combustion approach, Dahiya *et al.*,[35] have also studied the luminescence properties of Tb^{3+}-doped $BaLa_2ZnO_5$. Similarly, Xie *et al.*[36] have performed the synthesis and up-conversion luminescence properties of Ho^{3+}, Yb^{3+} co-doped $BaLa_2ZnO_5$ and observed that synthesized phosphors possess strong green and weak red up-conversion emissions centered at 548 nm, 664 nm, and 758 nm. Similarly, comparable studies of the structural and luminescent characteristics of Nd^{3+}, Tb^{3+}, and Eu^{3+} have also been done in other works.

From the above discussion, it is clear that several authors reported the synthesis of RE^{3+}-doped $BaLa_2ZnO_5$ phosphors by using combustion or sol–gel methods. It has also been found that in all the investigations, the luminescence studies have been carried out in either one of the three spectral regions—ultraviolet, visible, or near-infrared. Furthermore, none of the investigations have studied the distribution of ions using time-of-flight secondary ion mass spectrometry (ToF-SIMS) and the thermal behavior of the synthesized phosphor materials. In this work, an effort has been made to prepare Dy^{3+}-doped $BaLa_2ZnO_5$ phosphors by using a solid-state reaction method. The main aim was to determine its crystal structure and study the effect of different Dy^{3+} ion concentrations on the optical and luminescent properties of prepared phosphor materials. Comprehensive luminescence studies were carried out by recording the emission spectra in the ultraviolet, visible, and NIR regions. Additionally, the surface morphology, elemental composition, and ion distribution were also studied. The behavior of doping on the host was analyzed through the calculation of Judd–Ofelt intensity parameters. The thermal stability of the synthesized phosphor was analyzed through temperature-dependent luminescence spectra. The lifetime of the synthesized phosphor was computed from the decay profile. The detailed study has revealed that the synthesized $Ba(La_{2-x}Dy_x)ZnO_5$ (x = 0–7 mol%) phosphor can act as an efficient candidate for fabricating wLED for solid-state lighting applications.

Materials synthesis and characterization

A series of $Ba(La_{2-x}Dy_x)ZnO_5$ (x = 0–7 mol%) phosphor material was synthesized by using the solid-state reaction method. All the precursors employed, *i.e.*, $BaCO_3$ (99.9%), La_2O_3 (99.9%), ZnO (99.9%), and Dy_2O_3 (99.9%), were procured from Sigma Aldrich. Following the stoichiometric calculations, the required amount of all the precursors was thoroughly mixed in an agate mortar for several hours. During mixing, ethyl alcohol was added at regular intervals for proper homogenization. The mixture was then transferred to an alumina crucible and kept in a muffle furnace at 900 °C for 2 h with a heating and cooling rate of 5° min^{-1}. The mixture was removed from the furnace for further grinding and then calcinated at 1200 °C for 6 h with a heating and cooling rate of 5° min^{-1}. After calcination, the mixture was ground into a powder form of the desired nanomaterial.

The phase purity of the synthesized phosphor samples was confirmed using a Bruker AXS D8 Advanced X-ray Diffractometer (Cu-K_α) functioning at high resolution with a specific voltage and tube current of 40 kV and 40 mA, respectively. Band-

© 2023 The Author(s). Published by the Royal Society of Chemistry

Open Access Article. Published on 03 2023. Downloaded on 2025/5/31 23:29:15.
This article is licensed under a Creative Commons Attribution-NonCommercial 3.0 Unported Licence.

gap analysis was performed by recording the diffuse reflectance spectra using a PerkinElmer Lambda 950 spectrometer. Morphological and compositional measurements were performed using a JEOL JSM-7800F scanning electron microscope (SEM), equipped with an energy-dispersive X-ray spectroscopy (EDS) system. Time-of-flight secondary ion mass spectroscopy (ToF-SIMS 5) was employed for recording the surface maps displaying the distribution of ions. Photoluminescence spectra of synthesized phosphor material were recorded by using a Varian Carry-Eclipse fluorescence spectrophotometer coupled with a xenon lamp and photomultiplier tube (PMT) for excitation and recording PL spectra. Also, the He–Cd laser system with a 325 nm excitation wavelength was employed for recording the PL spectra in both the visible and NIR regions, along with temperature-dependent PL. Phosphorescence lifetime measurements were carried out using the FS5 fluorescence spectrophotometer.

Results and discussion

Phase purity and crystal structure

Fig. 1 represents the XRPD pattern of the synthesized series of $Ba(La_{2-x}Dy_x)ZnO_5$ (x = 0–7 mol%) phosphor. The obtained XRPD pattern was found to be consistent with the joint committee on powder diffraction standard (JCPDS) 01-080-1882 along with the crystallographic open database (COD) #2002571, thereby confirming the phase of synthesized phosphor material. From the JCPDS data file, it was found that the synthesized phosphor possesses a tetragonal phase structure with space group $I4/mcm$ (140) and lattice parameters $a = b = 6.9091$ Å and $c = 11.5907$ Å.

The absence of impurity peaks in the XRPD pattern at different doping concentrations established the fact that Dy^{3+} doping has not altered the basic crystal structure of $BaLa_2ZnO_5$.

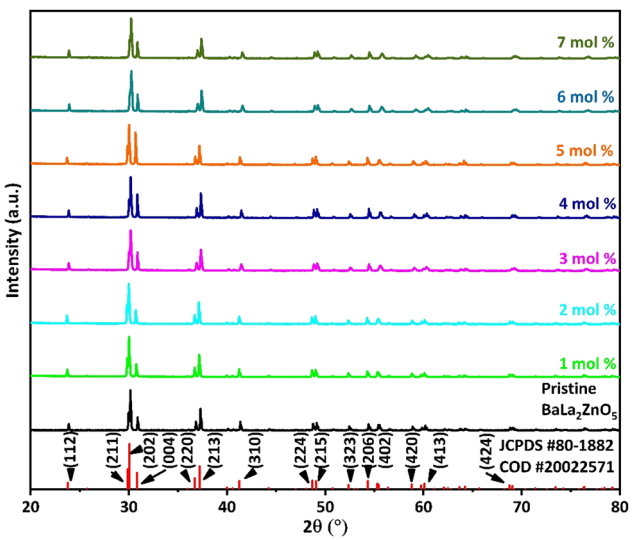

Fig. 1 X-ray powder diffraction pattern of $Ba(La_{2-x}Dy_x)ZnO_5$ (0–7 mol%) phosphor materials along with the standard diffraction pattern peaks pattern.

According to Vegard's mixing rule, dopant Dy^{3+} ions are supposed to replace La^{3+} ions in the host matrix. The replacement of the host lattice ion (La^{3+}) by the dopant lattice ions (Dy^{3+}) was validated by calculating the percentage radius difference (Δr) using the following formula:[37]

$$\Delta r = \frac{R_m(CN) - R_d(CN)}{R_m(CN)} \times 100 \quad (1)$$

In the above equation, R_m, R_d, and CN stand for effective ionic radii for host and dopant lattice ions along with their respective coordination numbers. By substituting the respective values in the above equation, the value of Δr was estimated to be 11.62, which is quite less than the acceptable limit of 30 percent.[38] The calculated value of Δr completely suggests the replacement of La^{3+} ions by Dy^{3+} ions, which is also evident by observing a slight shift in the XRPD pattern towards the right. Furthermore, other options for the replacement of Ba^{2+} and Zn^{2+} ions by the dopant Dy^{3+} ions are ruled out due to dissimilarity in their ionic radii and charges, which results in considerable percentage radii differences.[32]

In addition, the average crystallite size (D) of the synthesized phosphor was estimated by using the fundamental Scherrer's equation:[39]

$$D = \frac{0.941\lambda}{\beta \cos\theta} \quad (2)$$

In the above equation, D represents the grain size, λ represents the wavelength of the employed X-ray source (Cu-K_α radiation, λ = 0.154 nm), and β represents the value of the full-width half maxima (FWHM) of prominent peaks residing at angle θ. Applying the empirical formula, the average crystallite size was estimated to be 81.70 nm.

Band-gap analysis

For examining the effect of Dy^{3+}-doping on the optical properties of $BaLa_2ZnO_5$, diffuse reflectance spectra (DRS), depicted in Fig. 2(a), were recorded from 200 to 800 nm using a UV-visible spectrophotometer. From the figure, it is evident that at the initial concentrations of doping, the reflectance percentage slightly increases; however, as the concentration increases, a further decrease in the reflectance percentage from 80% to 60% is evident from the plot. A decrease in the reflectance percentage, in turn, tends to enhance the emission properties of the host. In addition, feeble peaks are evident in the reflectance plot for doped samples in the range of 290 nm to 480 nm, which has been ascribed to the intraconfigurational 4f transitions of Dy^{3+}-ions. Among the different peaks, two prominent peaks at 367.46 nm and 453.96 nm correspond to the $^6H_{15/2} \rightarrow {}^6P_{3/2,5/2}$ transitions of Dy^{3+}-ions, respectively.[32] The existence of weak peaks in the reflectance spectra highlights the practical application of the synthesized phosphor material for wLEDs.

Furthermore, for estimation of the bandgap, the obtained DRS spectra were subjected to a well-known theoretical approach called the Kubelka–Munk function. Correlating the Kubelka–Munk function and Tauc's generalization results in

Open Access Article. Published on 03 2023. Downloaded on 2025/5/31 23:29:15.
This article is licensed under a Creative Commons Attribution-NonCommercial 3.0 Unported Licence.

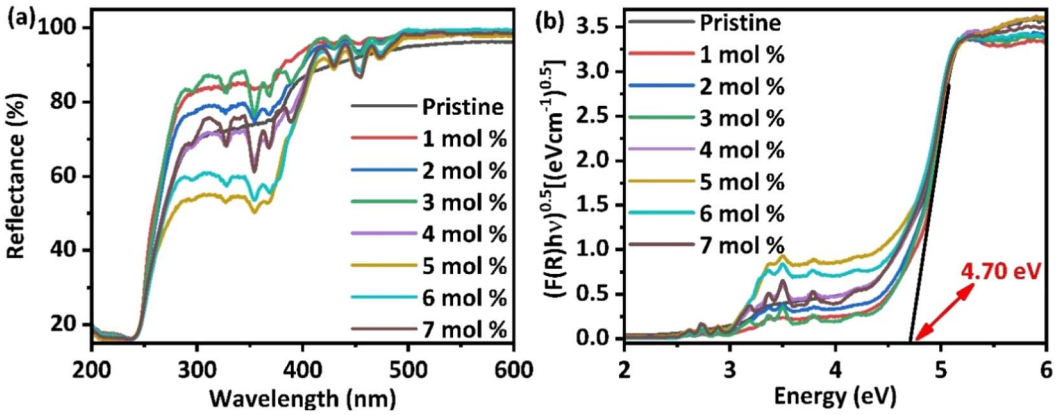

Fig. 2 (a) Diffusive reflectance spectra for $Ba(La_{2-x}Dy_x)ZnO_5$ (x = 0–7 mol%) phosphor (b) Tauc's plot for estimating the indirect bandgap of synthesized phosphor materials.

the general eqn (3) that helps in determining the nature of transitions.

$$[F(R_\infty)h\nu]^2 = C(h\nu - E_g)^n \quad (3)$$

In the above equation, C is constant, $F(R_\infty)$ represents the Kubelka–Munk function, $h\nu$ corresponds to the value of phonon energy, and n represents the type of electronic transition and can take values of either 1, 3 for direct allowed and forbidden transitions or 4, 6 for indirect allowed and forbidden transitions, respectively. It was observed that synthesized phosphor materials favor the occurrence of indirect allowed transitions. Fig. 2(b) represents Tauc's plot, from which it is evident that doping does not have to cause any significant change in the bandgap of the materials. The synthesized phosphor was found to have an indirect bandgap of the order of 4.70 eV, indicating that it belongs to the wide bandgap semiconductors and can be effectively used for different photonic, lasing, and optoelectronic applications.[40]

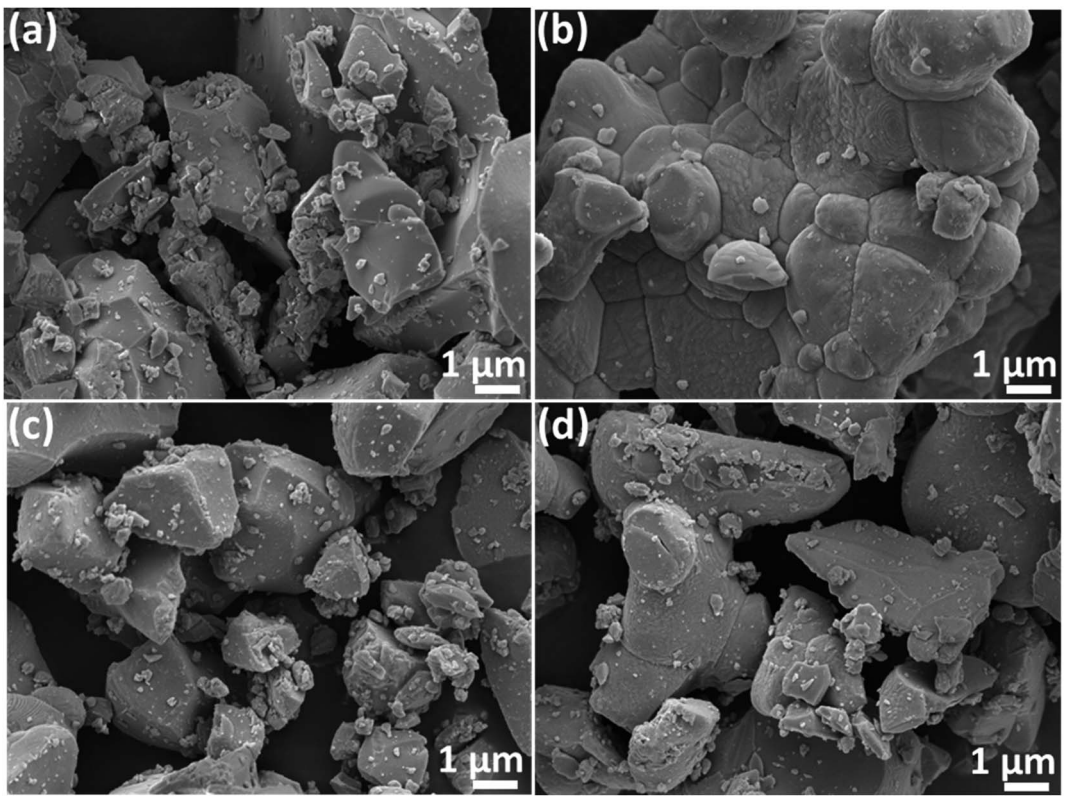

Fig. 3 SEM images for (a) 0 mol% of Dy^{3+} (b) 1 mol% of Dy^{3+} (c) 5 mol% of Dy^{3+} (d) 7 mol% of Dy^{3+} in $BaLa_2ZnO_5$ phosphor material.

© 2023 The Author(s). Published by the Royal Society of Chemistry

Open Access Article. Published on 03 2023. Downloaded on 2025/5/31 23:29:15.
This article is licensed under a Creative Commons Attribution-NonCommercial 3.0 Unported Licence.

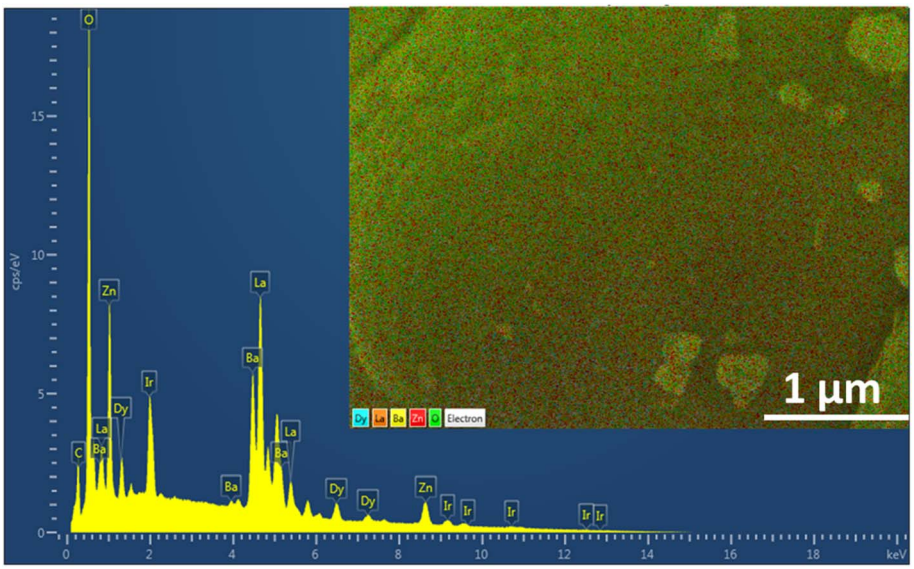

Fig. 4 EDS spectrum for 5 mol% doped $BaLa_2ZnO_5$ coated with Iridium.

Surface morphology and compositional probe

The progression in the microstructures of the $Ba(La_{2-x}Dy_x)ZnO_5$ phosphor material is depicted in Fig. 3. The different micrographs present in Fig. 3(a)–(d) correspond to the 0 mol%, 1 mol%, 5 mol%, and 7 mol% concentrations of the Dy^{3+} ion in the host. From the SEM micrographs, it is evident that surface morphology is strongly dependent on the activator concentration of Dy^{3+}. For the pristine sample, the SEM micrographs show uneven particle sizes and irregular shapes. However, at the initial doping concentrations, particles are completely agglomerating together, forming a sheet-like structure. As the doping concentrations increase, further particles start dispersing again in an irregular fashion. However, no such change in the structure is evident due to doping concentration. Also, to confirm the elemental composition, the EDS spectrum was recorded for the optimum doping concentration and is given in Fig. 4. The EDS spectrum validates the compositions, as the emission peaks present in the spectrum correlate with the Ba, La, Zn, O, and Dy.

TOF-SIMS analysis

ToF-SIMS images acquired for the pristine and doped samples (1, 5, and 7 mol%) are presented in Fig. 5(a)–(d). The images were recorded in a zone of 100 × 100 μm^2 and then combined overlays were created. These images reveal the topography of the synthesized powder. All the images depicted were recorded after the sputter-cleaning process. The overlay mapping images depict the regular distribution of different ions on the surface. Besides visualizing the distribution of the host ions, *i.e.*, Ba, La, Zn, and O, it is evident that Dy^{3+}-ions have been successfully incorporated into the host lattice. As can be seen from the figures, all the ions present in the host are dispersed consistently in each sample. In addition, the dopant Dy^{3+} ions also seem to be present throughout the sample's surface.[8]

Photoluminescence study

Photoluminescence excitation (PLE) and emission (PL) spectra recorded from 200 nm to 800 nm of the synthesized $Ba(La_{2-x}Dy_x)ZnO_5$ (x = 1–7 mol%) phosphor materials are depicted in Fig. 6. In the recorded spectra (PLE and PL), there are many peaks because of the intraconfigurational f–f transitions of the Dy^{3+} ion. The PLE spectra (Fig. 6(a) and (b)) were recorded at an emission wavelength of 577 nm, and the emission was found to consist of a broad charge transfer band (CTB), followed by several peaks at 294.44, 326.67, 352.87, 367.98, 388.37, 429.13, 453.89, and 472.77 nm, which correspond to $^6H_{15/2} \rightarrow {}^4K_{13/2}$, $^6H_{15/2} \rightarrow {}^6P_{3/2}$, $^6H_{15/2} \rightarrow {}^6P_{7/2}$, $^6H_{15/2} \rightarrow {}^6P_{5/2}$, $^6H_{15/2} \rightarrow {}^4I_{13/2}$, $^6H_{15/2} \rightarrow {}^4G_{11/2}$, $^6H_{15/2} \rightarrow {}^4I1_{5/2}$, and $^6H_{15/2} \rightarrow {}^4F_{9/2}$, respectively.

Similarly, while observing the PL spectrum (Fig. 6(c) and (d)) recorded at an excitation wavelength of 352 nm, it consists of two sharp emission peaks at 486.52 (blue) and 576.95 (yellow), which correspond to $^4F_{9/2} \rightarrow {}^6H_J$ (J = 15/2, 13/2), respectively.[41,42] In addition, there exist two feeble peaks in the PL spectra at 669.49 and 755.62 nm, which correspond to $^4F_{9/2} \rightarrow {}^6H_{11/2}$. For analyzing the emission in the NIR, the emission spectrum for the optimum doping concentration was recorded from 300 to 1600 nm by using a UV excitation 325 nm PL laser system, which is depicted in Fig. 7.

The emission spectra recorded by the PL laser system (Fig. 7(a)) are similar to those presented in Fig. 6(c) and (d), thereby further illustrating the observed spectra. However, the emission spectrum of the synthesized phosphor in the NIR region (Fig. 7(b)) possesses two sharp peaks at 920 nm and 1090 nm and two feeble peaks around 1260 nm and 1426 nm. These two sharp peaks correspond to the transitions from $^4F_{9/2} \rightarrow {}^6F_J$ (J = 7/2, 9/2), respectively.[43]

The most peculiar thing to observe in the emission spectrum of synthesized phosphor is that all the emissions mostly arise from the $^4F_{9/2}$ energy level to different ground state levels. The

Open Access Article. Published on 03 2023. Downloaded on 2025/5/31 23:29:15.
This article is licensed under a Creative Commons Attribution-NonCommercial 3.0 Unported Licence.

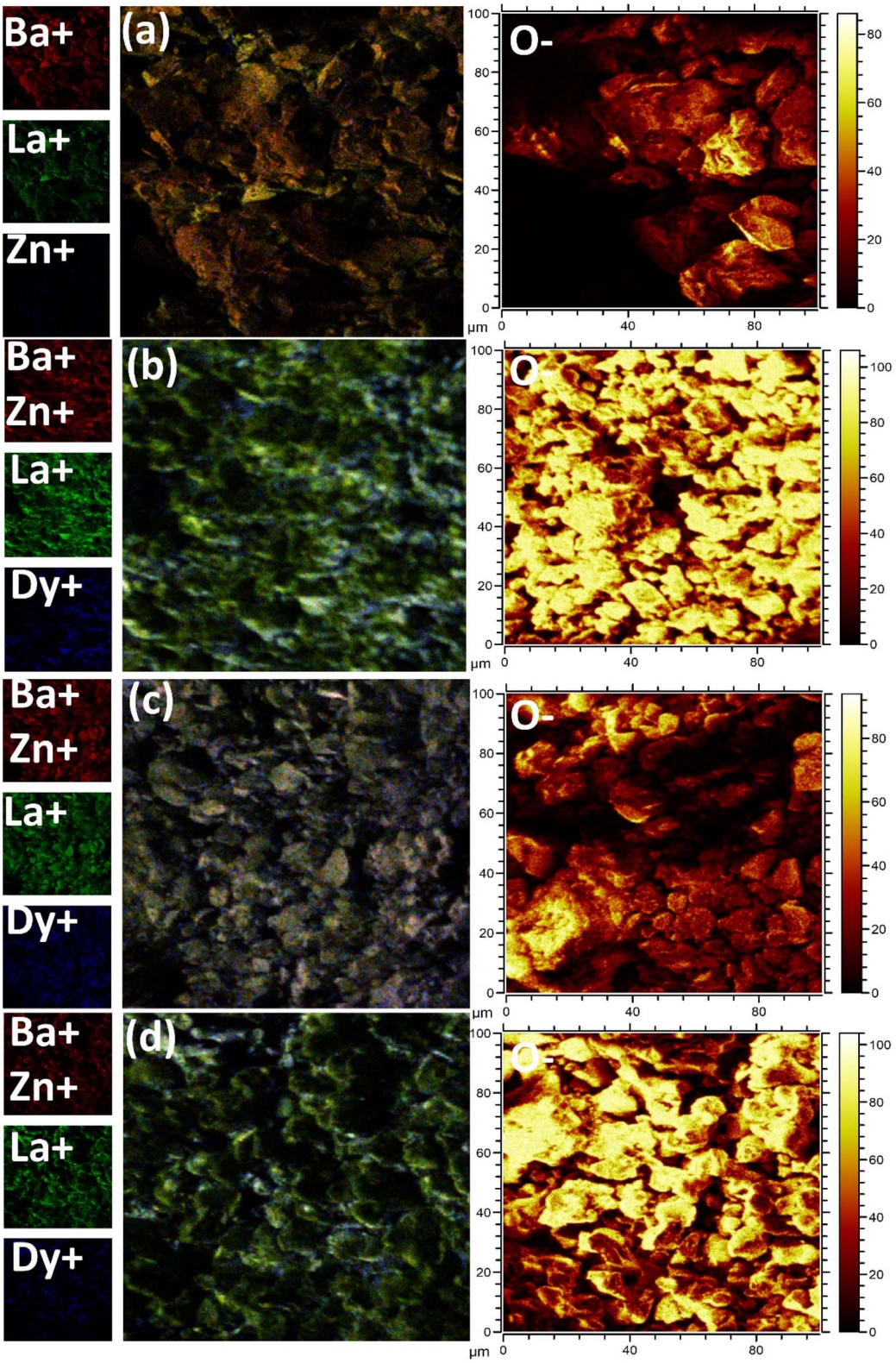

Fig. 5 TOF-SIMS surface mapping for (a) undoped (b) 1 mol%, concentrations (c) 5 mol% , and (d) 7 mol% concentations of Dy^{3+} in $Ba(La_{2-x}Dy_x)ZnO_5$ phosphor.

different transitions involved in the emission from UV to NIR regions are well depicted in the energy level diagram shown in Fig. 8. During the early phase of excitation, the electrons residing in the ground state get stimulated into different excited states. From the different excitations these electrons reach the stable quantum mechanical state $^4F_{9/2}$ *via* non-radiative

© 2023 The Author(s). Published by the Royal Society of Chemistry

Open Access Article. Published on 03 2023. Downloaded on 2025/5/31 23:29:15.
This article is licensed under a Creative Commons Attribution-NonCommercial 3.0 Unported Licence.

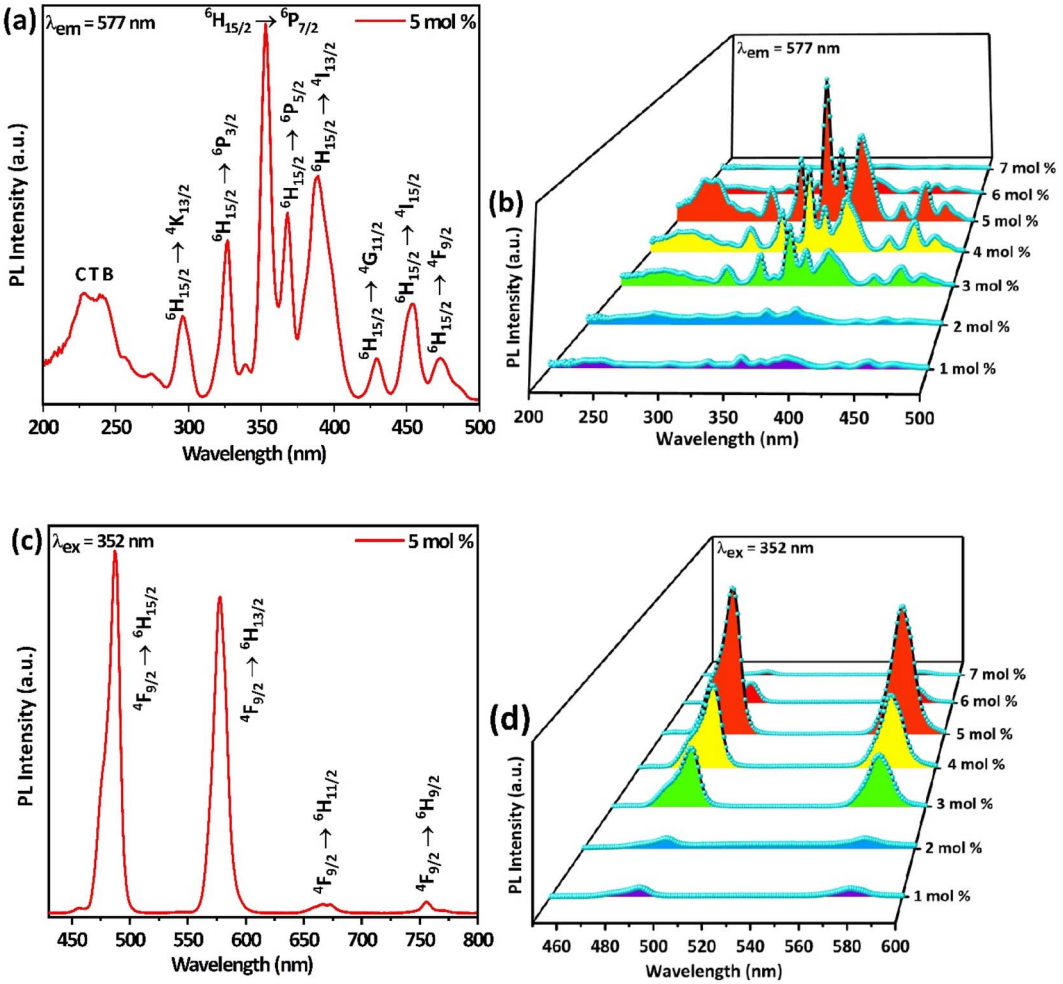

Fig. 6 (a and b) Excitation spectra of $Ba(La_{2-x}Dy_x)ZnO_5$ ($x = 5$ mol%) and 3D-excitation plot for $Ba(La_{2-x}Dy_x)ZnO_5$ ($x = 1$–7 mol%), recorded at an emission wavelength of 577 nm. (c and d) Emission spectra of $Ba(La_{2-x}Dy_x)ZnO_5$ ($x = 5$ mol%) and 3D-emission plot for $Ba(La_{2-x}Dy_x)ZnO_5$ ($x = 1$–7 mol%), recorded at an excitation wavelength of 352 nm.

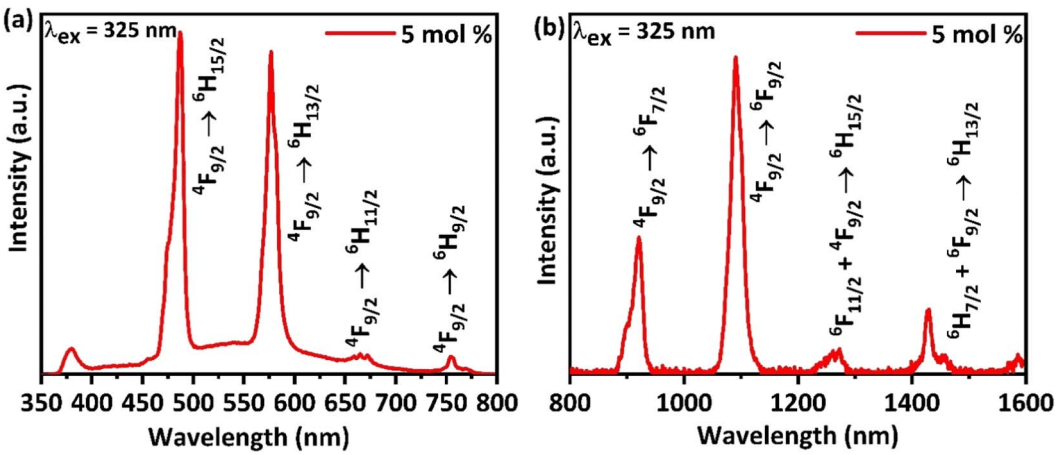

Fig. 7 (a) Emission spectra of $Ba(La_{2-x}Dy_x)ZnO_5$ ($x = 5$ mol%) from UV to visible and (b) visible to NIR regions of the electromagnetic spectrum recorded by using an excitation wavelength of 325 nm.

Open Access Article. Published on 03 2023. Downloaded on 2025/5/31 23:29:15.
This article is licensed under a Creative Commons Attribution-NonCommercial 3.0 Unported Licence.

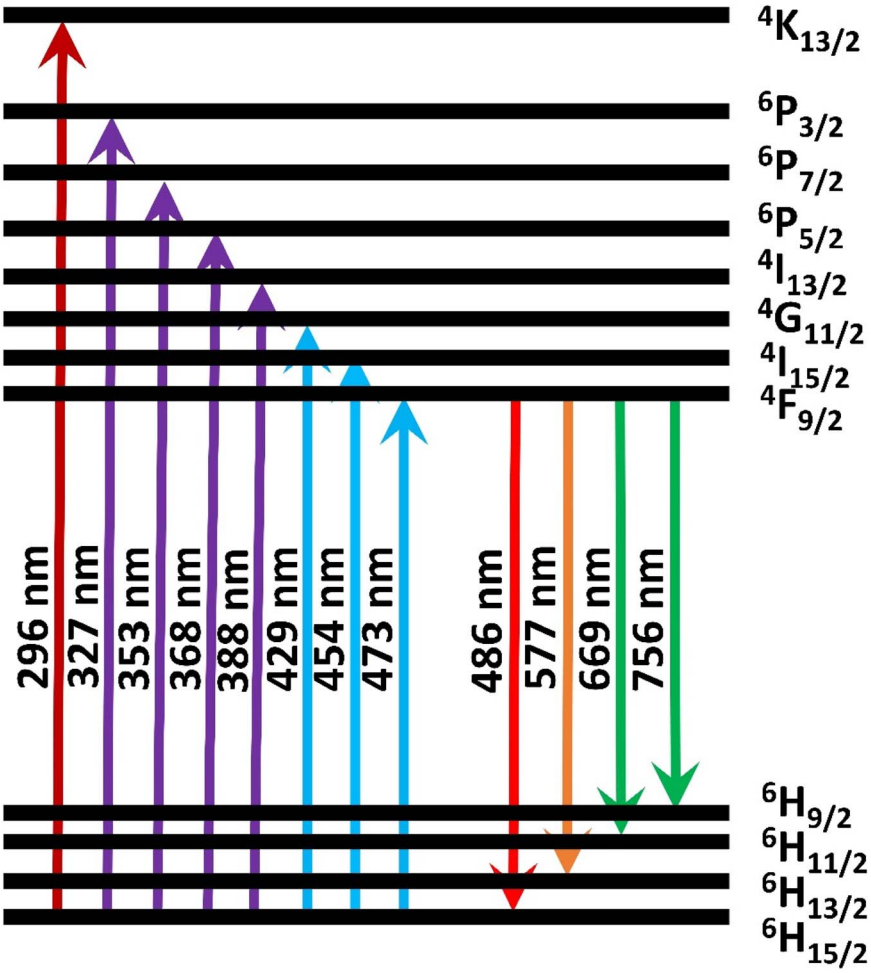

Fig. 8 Energy level diagram corresponding to the excitation and emission spectra of Dy^{3+} activated $BaLa_2ZnO_5$.

transitions. Finally, the blue and yellow emission transitions occur from the stable $^4F_{9/2}$ state to different ground-state energy levels.

The impact of doping on the host materials is evident from the varying PLE and PL intensities (Fig. 6(c) and (d) and 9(a)). Although all the profiles are similar, a gradual increase in intensity is observed until the amount of doping acquires a 5 mol% value, after which a significant drop in intensity is observed. The decrease in intensity is caused by the concentration quenching (CQ) phenomenon, which may be the result

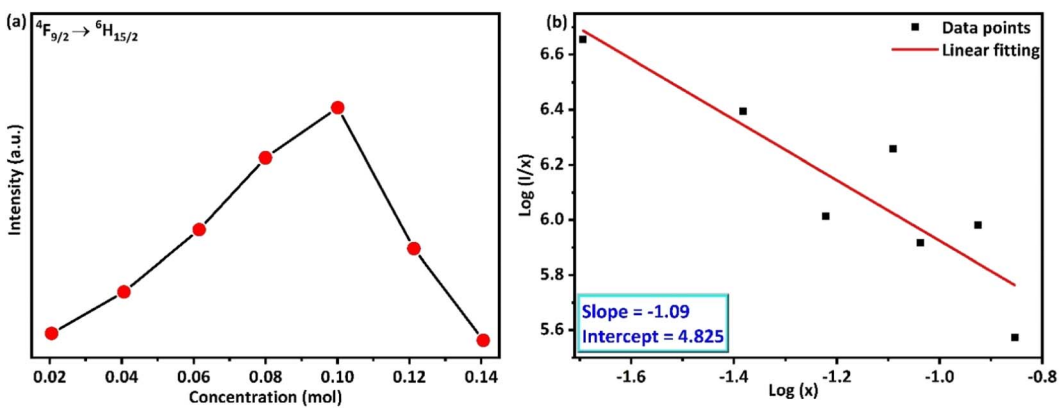

Fig. 9 (a) Variation of emission intensity ($^4F_{9/2} \rightarrow {}^6H_{15/2}$) with variation in the doping concentration (b) logarithmic variation of the PL intensity of Dy^{3+} doped $BaLa_2ZnO_5$ phosphor.

© 2023 The Author(s). Published by the Royal Society of Chemistry

Open Access Article. Published on 03 2023. Downloaded on 2025/5/31 23:29:15.
This article is licensed under a Creative Commons Attribution-NonCommercial 3.0 Unported Licence.

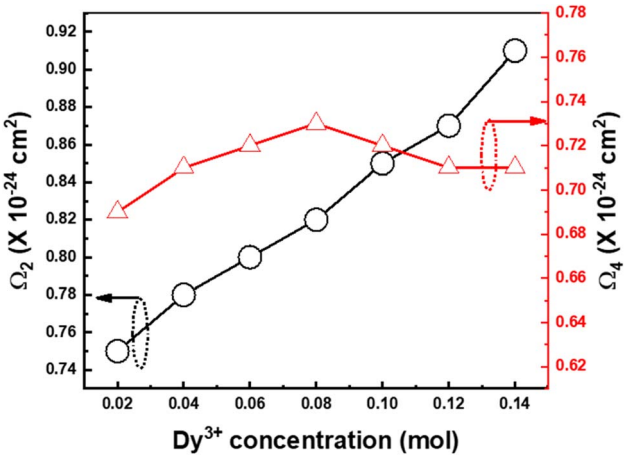

Fig. 10 Variation of Ω_2 and Ω_4 for Ba(La$_{2-x}$Dy$_x$)ZnO$_5$ (x = 1–7 mol%) host matrix.

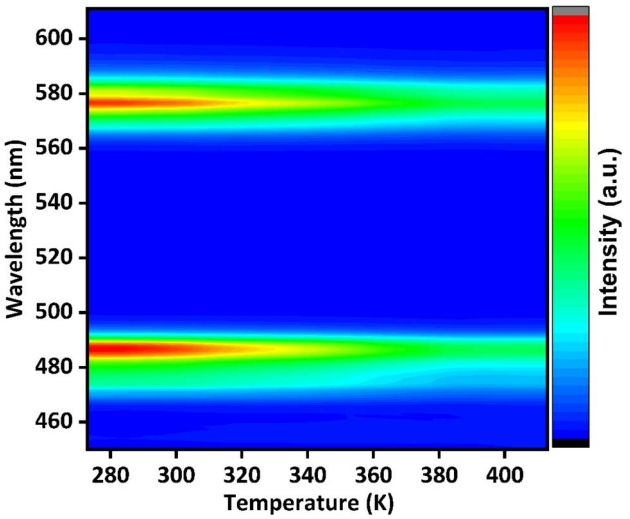

Fig. 11 Temperature-dependent photoluminescence spectra of Ba(La$_{2-x}$Dy$_x$)ZnO$_5$ (x = 5 mol%) phosphor.

of non-radiative (nR) cross-relaxation processes. The validation of the nR cross-relaxation process can be done by calculating the value of the critical distance (R_c) using Blasse's equation:[44]

$$R_c = 2\left(\frac{3V}{4\pi XN}\right)^{\frac{1}{3}} \quad (4)$$

In the above equation, V stands for the volume of the unit cell, X represents the value of the optimal doping concentration, and N stands for the number of replaceable cations. By substituting the respective values in the above equation, we get a value of R_c = 13.82 Å, which is quite larger than the acceptable value of 5 Å, thereby ruling out the possibility of CQ through nR cross-relaxation pathways.[45] Therefore, the phenomenon of CQ can either be due to radiative reabsorption or multipolar interaction phenomena. However, there is no evidence of overlap between the excitation and emission, which thereby clearly infers the non-occurrence of radiative reabsorption processes.[32] Thus, the effective pathway for CQ is due to multipolar interactions, which can be assessed by using Dexter's generalization.[46,47] The amount of energy being transferred is governed by the extent of interaction between the luminescence centers. While studying the CQ phenomenon, Huang *et al.*,[48] found that the interaction between the luminescence centers has a strong correlation with the luminescence intensity and doping concentration. The relation between them can be well understood from Huang's equation:[48]

$$I = \alpha^{1-\frac{s}{3}}\Gamma\left(1+\frac{s}{3}\right) \quad (5)$$

$$\alpha = x\Gamma\left(1-\frac{s}{3}\right)\left[X_o\left(1+\frac{A}{\gamma}\right)\right]^{\frac{3}{s}} \quad (6)$$

In the above eqn (5) and (6), I stand for peak intensity corresponding to the optimal doping concentration value x, and s represents the type of interaction, which can be either dipole–dipole (s = 6), dipole–quadruple (s = 8), or quadruple–quadruple (s = 10). Γ corresponds to the probability of the occurrence of donor intrinsic transitions. Inference about the type of interaction can be estimated by solving the above eqn (5) and (6), which result in the following general equation:[49]

$$\log\frac{I}{x} = \left[-\frac{s}{3}\log x + \log f\right] \quad (7)$$

In the above equation, f is a constant, and I represent the intensity corresponding to the different concentrations of doping (Dy^{3+}). The term "$-s/3$" in the above equation represents the slope of the graph plotted in between log(I/x) *vs.* log(x) and was estimated to be −1.09 (Fig. 9(b)). Therefore, the measured value of s was found to be 3.27, which suggests the only option for the energy transfer and subsequent CQ phenomenon is the occurrence of some exchange-type interaction within the synthesized phosphor.[32] As the concentration of Dy^{3+} ions exceeds its optimum values, the space between the activator ions starts decreasing, which results in the initiation of some non-radiative exchange-type of interactions. As a result, a decrease in emission intensity is observed. All the above-discussed photoluminescence results are also endorsed by the DRS spectra results discussed above.

Judd–Ofelt analysis

For understanding the variation in the intensities of the blue and yellow bands, optimization of radiative transfer was done by employing the Judd–Ofelt (JO) theory.[50,51] The line strength of the activator ions was computed from the excitation spectra using the magnetic dipole (MD) and electric dipole (ED) transitions. The probability of occurrence for ED transitions is higher than that of MD transitions.[52] Luo *et al.*[53] have envisaged a simplistic approach for determining the JO parameters for powder samples based on their excitation spectra. The same approach was put to use on many systems, and it was found that the computed results are in good agreement with the results obtained *via* the conventional method. Dutta *et al.*[52] have also reported a comprehensive formalism for the estimation of the

Open Access Article. Published on 03 2023. Downloaded on 2025/5/31 23:29:15.
This article is licensed under a Creative Commons Attribution-NonCommercial 3.0 Unported Licence.

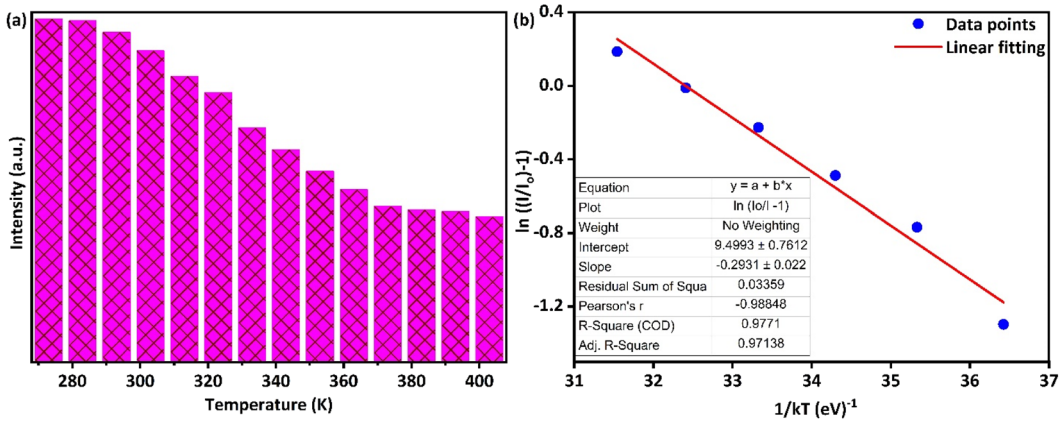

Fig. 12 (a) Bar chart plot depicting the variation of emission intensity with an increase in temperatures (b) Arrhenius plot for estimation of the activation energy of synthesized $Ba(La_{2-x}Dy_x)ZnO_5$ ($x = 5$ mol%) phosphor.

JO parameters using the excitation spectra. In the current study, a similar formalization was opted for when computing the line strength:

$$S_{\text{Cal}}^{\text{ed}}\left(J \rightarrow J'\right) = \sum \Omega_t |\langle \psi' | U^t | \psi' \rangle|^2 \quad (8)$$

Here, $|U^t|$ represents the unit tensor operator, Ω_2, Ω_4, and Ω_6 denote the JO intensity parameters. These parameters provide information about the impact of the host on the plausibility of the transition. Furthermore, employing the excitation spectra, experimental line strengths were also calculated using the following eqn (9):

$$S_{\text{meas}}^{\text{ed}}\left(J \rightarrow J'\right) = \frac{3hc(2J+1)}{8\pi^3 \bar{\lambda} e^2 N_o} \frac{9n}{(n^2+2)^2} G_{\text{exc}} \quad (9)$$

J and J' represent the angular momentum quantum numbers corresponding to the ground and excited states. n is the value of the refractive index of the sample, and G_{exc} is computed from the integral excitation intensity. Thereafter, for computing the JO parameters, the least squares fitting method was employed between the calculated and experimental line strengths. The deviation among them was calculated using the root mean square (rms) parameters

$$\text{rms}\Delta S = \sqrt{\sum_{i=1}^{N} (S_{\text{meas}} - S_{\text{cal}})^2 \Big/ N - 3} \quad (10)$$

where N corresponds to the band number. The computed JO parameters for different concentrations of $Ba(La_{2-x}Dy_x)ZnO_5$ ($x = 1$–7 mol%) were plotted as shown in Fig. 10. According to the existing literature, the Ω_2 value of 5 mol% Dy^{3+}-doped $BaLa_2ZnO_5$ phosphor was found to be comparatively low, *i.e.*, 0.82×10^{-24} cm^2.[52] The low value of Ω_2 pointed to the high symmetry of the ligand environment surrounding Dy^{3+} ions. When the concentration of Dy^{3+} increased, it was found that the Ω_2 value of the Dy^{3+}-doped $BaLa_2ZnO_5$ phosphor changed slightly, modifying its covalent nature due to the overlap of molecular orbitals between O^{2-} ion (p-orbital) and Dy^{3+} (f-orbital). The electron cloud extended as a result of the orbital overlap, creating a connection with a stronger covalent character. According to the JO analysis, Dy^{3+} ion placement follows inversion symmetry. The variation of Ω_4 parameters with Dy^{3+}

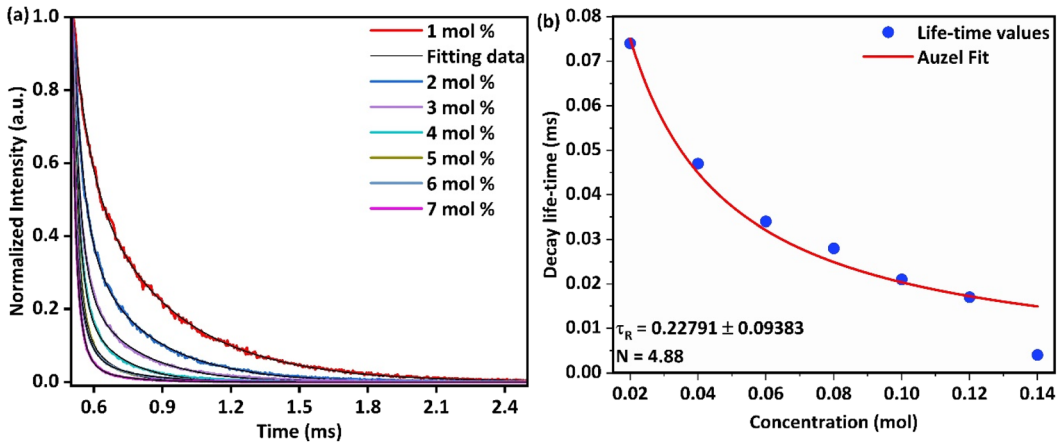

Fig. 13 Luminescence decay curves of synthesized $Ba(La_{2-x}Dy_x)ZnO_5$ phosphor ($x = 1$–7 mol%) (b) Auzel's fitting for calculation of the intrinsic radiative lifetime of the synthesized phosphor material.

© 2023 The Author(s). Published by the Royal Society of Chemistry

Open Access Article. Published on 03 2023. Downloaded on 2025/5/31 23:29:15.
This article is licensed under a Creative Commons Attribution-NonCommercial 3.0 Unported Licence.

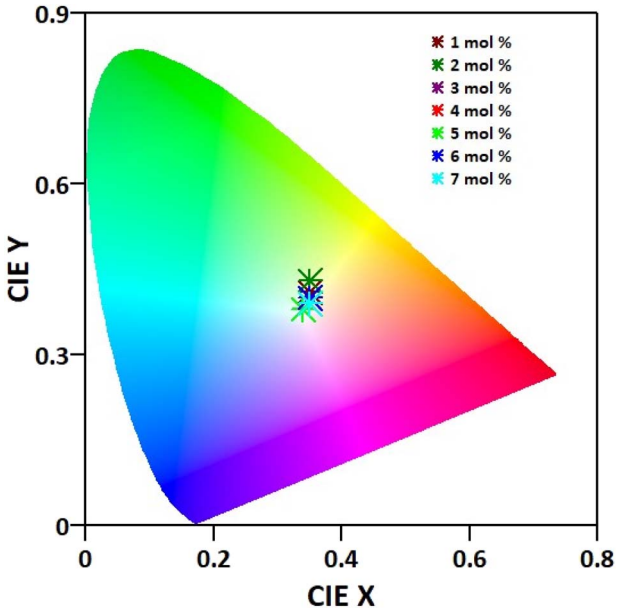

Fig. 14 Chromaticity diagram depicting the variation in the color coordinates as the concentration of Dy^{3+} changes from 1 to 7 mol% in the synthesized $Ba(La_{2-x}Dy_x)ZnO_5$ phosphor.

concentration was observed to be almost negligible, indicating the strong symmetric nature of Dy^{3+} ions in the present host. Owing to this excellently symmetric nature, blue and yellow emissions can provide near-white emissions from the present phosphor materials.

Thermal stability

The thermal stability parameter is another prominent factor in determining the effectiveness of phosphor materials. In this regard, temperature-dependent PL emission of $Ba(La_{2-x}Dy_x)ZnO_5$ ($x = 5$ mol%) was recorded by using Kimmon IK Series 325 nm Laser Source excitation from room temperature to 410 K, and the variation in intensity observed is depicted in Fig. 11.

It is evident from Fig. 11 that the position of emission bands did not change as the temperature increased from room temperature to 410 K. This invariability of the emission peak position helps in recording the steady-state emission even at elevated temperatures. However, an increase in temperature tends to decrease the intensity of PL emission, as is evident from Fig. 11 and 12(a), due to different temperature quenching processes.[54] Fig. 12(a) represents the variation of intensity with the rise in temperature. The total variation in intensity can be divided into three temperature regions: 273–313 K, 323–373 K, and 383–403 K, respectively. As the temperature increases from room temperature, a slight variation in intensity is observed, suggesting a stable thermal behavior up to 313 K. However, in the second region (323–373 K), a gradual decrease in intensity is observed, which again stabilizes after 383 K. Beyond that, the PL intensity shows stabilized behavior up to 403 K, which confirms the good thermal stability of the synthesized phosphor. The essence of thermal quenching, due to which the gradual decrease in intensity occurs from 323 to 373 K, can be observed by determining the activation energy using the following equation:[55]

$$\ln\left(\frac{I_o}{I} - 1\right) = \ln A - \frac{\Delta E}{kT} \quad (11)$$

In the above equation, I_o represents the intensity at room temperature, I denotes the emission intensity at different temperatures (T), A is constant, ΔE signifies activation energy, and k stands for the Boltzmann constant. Fig. 12(b) represents the curve corresponding to $\ln(I_o/I - 1)$ *versus* $1/kT$ for $Ba(La_{2-x}Dy_x)ZnO_5$ ($x = 5$ mol%) phosphor. The slope for the plot was estimated through linear fitting and is around −0.29, revealing that the value of activation energy is 0.29 eV for synthesized $Ba(La_{2-x}Dy_x)ZnO_5$ ($x = 5$ mol%) phosphors. Obtained activation energy endorses excellent thermal stability and its applicability in high-power wLEDs and other applications.[54]

Lifetime and photometric analysis

The phenomenon of energy transfer can be further evaluated by analyzing the decay curves. The decay curves depicted in Fig. 13(a) were recorded using an excitation and emission wavelength of 352 nm and 577 nm, respectively. It was observed that all the curves were not following the single exponential trend, which can be attributed to the unequal distribution of dopant ions in the host matrix.[19] Thus, the decay curves were fitted by the double exponential function:[56]

$$I(t) = I_o + A_1 \exp^{-t/\tau_1} + A_2 \exp^{-t/\tau_2} \quad (12)$$

Table 1 Fitting parameters and the calculated average lifetime values for varying doping concentrations of Dy^{3+} in synthesized $Ba(La_{2-x}Dy_x)ZnO_5$ phosphor materials

Concentration (mol%)	Adj R^2 value	Chi-square value ($\times 10^{-6}$)	Average lifetime (ms)
1	0.9994	6.00	0.074
2	0.9994	3.39	0.047
3	0.9993	2.05	0.034
4	0.9995	1.17	0.028
5	0.9056	175	0.021
6	0.9998	0.27	0.017
7	0.9999	0.12	0.004

Open Access Article. Published on 03 2023. Downloaded on 2025/5/31 23:29:15.
This article is licensed under a Creative Commons Attribution-NonCommercial 3.0 Unported Licence.

Table 2 Chromaticity coordinates and other parameters correspond to the different concentrations of Dy^{3+} ions in the host matrices $BaLa_2ZnO_5$

$BaLa_{2-x}Dy_xZnO_5$ (mol%)	CIE coordinates (x, y)	(u', v')	CCT (K)
1	0.3549, 0.4145	0.1954, 0.5135	4887
2	0.3525, 0.4331	0.1882, 0.5203	4998
3	0.3463, 0.3859	0.5006, 0.0158	5058
4	0.3463, 0.3923	0.1977, 0.5034	5061
5	0.3448, 0.3836	0.1995, 0.4994	5102
6	0.3480, 0.4041	0.1958, 0.5074	5029
7	0.3508, 0.3971	0.1987, 0.5059	4951

In the above eqn (12), $I(t)$ represents emission intensity at some time (t), I_o represents the background intensity, A_1 and A_2 are constants, and τ_1 and τ_2 correspond to lifetimes for different decays, respectively. The average lifetime was calculated using the following equation:

$$\tau = \frac{A_1\tau_1^2 + A_2\tau_2^2}{A_1\tau_1 + A_2\tau_2} \quad (13)$$

Employing the above eqn (13), it was observed that the average lifetime of the synthesized phosphor decreases from 0.074 ms to 0.004 ms (Table 1) as the concentration of Dy^{3+} varies from 1 to 7 mol% due to the nR energy relocation phenomenon.

The observed decrease in a lifetime with the increase in the concentration of Dy^{3+} was further assessed through Auzel's model (Fig. 13(b)) by using the following equation:

$$\tau(c) = \frac{\tau_R}{1 + \frac{c}{c_o}\exp^{\frac{-N}{3}}} \quad (14)$$

Here, c represents the variable concentration of the dopant ions in terms of mol%, $\tau(R)$ represents the intrinsic lifetime, and N represents the total number of photons generated during the relaxation of the $^4F_{9/2}$ state to different ground states *via* nR processes. Furthermore, $^4F_{9/2}$ is the only stable quantum mechanical state in Dy^{3+} and is responsible for other radiative relaxations with a radiative lifetime $\tau(R)$ of 0.23 ms.

The CIE paradigm of the synthesized $Ba(La_{2-x}Dy_x)ZnO_5$ phosphor is depicted in Fig. 14. The chromaticity coordinates and other parameters like (u', v') (Table 2) were calculated as per the standards of the Commission Internationale de l'Eclairage (CIE). Also employing the McCamy formula,[57] the CCT values of the synthesized materials were also computed and were found to vary from 4887 to 5102 K, as shown in Table 1. From the different parameters listed in Table 2, it is evident that the synthesized phosphor material exhibits white emission coordinates. For the optimal doping concentration, these coordinates approximately match the National TV Standards Committee (NTSC) standards ($x = 0.333, y = 0.0333$) and are in accord with the available literature.[8,19,32] These findings suggest that the as-synthesized phosphor materials can be suitable for the generation of UV-excited warm white light emission.

Conclusion

In summary, a Dy^{3+}-activated $BaLa_2ZnO_5$ phosphor material emitting a white light was synthesized through a high-temperature solid-state reaction. The XRPD pattern confirms the tetragonal-phase transparency as well as the structural stability of the synthesized nanomaterial when doped with Dy^{3+} ions. Diffusive reflectance spectra were recorded for computing the bandgap, and it was found that the synthesized phosphor possesses an indirect bandgap of the order of 4.70 eV. It was found that doping does not have a significant impact on the morphology of the particles. Under the excitation and emission wavelengths of 325 nm, 352 nm, and 577 nm, the photoluminescence spectra of targeted samples were analyzed to elucidate the incorporation of Dy^{3+} ions in the $BaLa_2ZnO_5$ host matrix. The emission spectra were found to consist of two sharp blue and yellow bands, which are responsible for the white emission exhibited by the synthesized phosphor material. Furthermore, an upsurge in luminescence intensity was observed until the concentration of Dy^{3+} reached 5 mol%. After that, the intensity decreases due to the CQ phenomenon initiated by the exchange type of interaction. The thermal stability of the synthesized phosphor was also assessed from temperature-dependent photoluminescence spectra for optimal doping, and it was found that the synthesized phosphor has good thermal stability and possesses an activation energy of 0.29 eV. The decay lifetime of synthesized phosphor ranges in microseconds and shows a decreasing trend with an increase in doping concentrations of Dy^{3+}. The obtained lifetime was fitted with Auzel's model, and a radiative lifetime of the order of 0.23 ms was attained for the stable $^4F_{9/2}$ quantum mechanical state. Lastly, the CIE coordinates of the synthesized phosphor were found to lie in the white region of the color gamut. The chromaticity coordinates (0.3448, 0.3836) for the optimal doping with CCT 5102 K was found to match well with NTSC standards. In a nutshell, the synthesized phosphor material is capable of being used effectively for fabricating wLEDs for solid-state lighting applications.

Conflicts of interest

There are no conflicts to declare.

© 2023 The Author(s). Published by the Royal Society of Chemistry

Open Access Article. Published on 03 2023. Downloaded on 2025/5/31 23:29:15.
This article is licensed under a Creative Commons Attribution-NonCommercial 3.0 Unported Licence.

Acknowledgements

VK acknowledges the "Fund for Improvement of S&T Infrastructure (FIST)" of the Department of Science & Technology (DST), Government of India (Grant No. SR/FST/PS-1/2021/169), for the financial support provided to the Department of Physics, National Institute of Technology Srinagar, India. This work is also based on the research supported by the South African Research Chairs Initiative of the Department of Science and Technology and the National Research Foundation of South Africa (grand 84415). The financial assistance of the National Research Foundation (NRF) and the University of the Free State towards this research is hereby acknowledged.

References

1 J. McKittrick and L. E. Shea-Rohwer, Review: Down Conversion Materials for Solid-State Lighting, *J. Am. Ceram. Soc.*, 2014, **97**, 1327–1352, DOI: **10.1111/JACE.12943**.

2 G. B. Nair, H. C. Swart and S. J. Dhoble, A review on the advancements in phosphor-converted light emitting diodes (pc-LEDs): Phosphor synthesis, device fabrication, and characterization, *Prog. Mater. Sci.*, 2020, **109**, 100622, DOI: **10.1016/J.PMATSCI.2019.100622**.

3 V. Kumar, S. Som, S. Dutta, S. Das and H. C. Swart, Red-light-emitting inorganic La_2CaZnO_5 frameworks with high photoluminescence quantum efficiency: Theoretical approach, *Mater. Des.*, 2016, **93**, 203–215, DOI: **10.1016/j.matdes.2015.12.153**.

4 H. Hu and W. Zhang, Synthesis and properties of transition metals and rare-earth metals doped ZnS nanoparticles, *Opt. Mater.*, 2006, **28**, 536–550, DOI: **10.1016/J.OPTMAT.2005.03.015**.

5 S. Sheoran, V. Singh, S. Singh, S. Kadyan, J. Singh and D. Singh, Down-conversion characteristics of Eu^{3+} doped $M_2Y_2Si_2O_9$ (M = Ba, Ca, Mg and Sr) nanomaterials for innovative solar panels, *Prog. Nat. Sci.: Mater. Int.*, 2019, **29**, 457–465, DOI: **10.1016/J.PNSC.2019.07.003**.

6 U.S. Department of Energy, *Energy savings forecast of SSL in general illumination applications*, 2019, DOI: **10.2172/1374119**.

7 S. Ray, P. Tadge, S. Dutta, T. M. Chen, G. B. Nair and S. J. Dhoble, Synthesis, luminescence and application of $BaKYSi_2O_7:Eu^{2+}$ A new blue-emitting phosphor for near-UV white-light LED, *Ceram. Int.*, 2018, **44**, 8334–8343, DOI: **10.1016/J.CERAMINT.2018.02.022**.

8 S. Verma, D. Kumar, S. Dutta, V. Sharma, H. C. Swart and V. Kumar, A novel near white light emitting phosphor $KSrYSi_2O_7:Dy^{3+}$ Synthesis, characterization and luminescence properties, *Vacuum*, 2020, **174**, 109179, DOI: **10.1016/j.vacuum.2020.109179**.

9 J. McKenna, A look ahead to the 2015 International Year of Light and Light-based Technologies, *J. Opt.*, 2014, **16**, 120201, DOI: **10.1088/2040-8978/16/12/120201**.

10 C. Y. Sun, X. L. Wang, X. Zhang, C. Qin, P. Li, Z. M. Su, D. X. Zhu, G. G. Shan, K. Z. Shao, H. Wu and J. Li, Efficient and tunable white-light emission of metal–organic frameworks by iridium-complex encapsulation, *Nat. Commun.*, 2013, **41**(4), 1–8, DOI: **10.1038/ncomms3717**.

11 N. Srinivasa Rao, S. Dhamodaran, A. P. Pathak, P. K. Kulriya, Y. K. Mishra, F. Singh, D. Kabiraj, J. C. Pivin and D. K. Avasthi, Structural studies of Ge nanocrystals embedded in SiO_2 matrix, *Nucl. Instrum. Methods Phys. Res., Sect. B*, 2007, **264**, 249–253, DOI: **10.1016/J.NIMB.2007.08.094**.

12 A. J. Kenyon, Recent developments in rare-earth doped materials for optoelectronics, *Prog. Quantum Electron.*, 2002, **26**, 225–284, DOI: **10.1016/S0079-6727(02)00014-9**.

13 Y. C. Li, Y. H. Chang, Y. F. Lin, Y. S. Chang and Y. J. Lin, Synthesis and luminescent properties of Ln^{3+} (Eu^{3+}, Sm^{3+}, Dy^{3+})-doped lanthanum aluminum germanate $LaAlGe_2O_7$ phosphors, *J. Alloys Compd.*, 2007, **439**, 367–375, DOI: **10.1016/J.JALLCOM.2006.08.269**.

14 S. Som, P. Mitra, V. Kumar, V. Kumar, J. J. Terblans, H. C. Swart and S. K. Sharma, The energy transfer phenomena and colour tunability in $Y_2O_2S:Eu^{3+}/Dy^{3+}$ micro-fibers for white emission in solid state lighting applications, *Dalton Trans.*, 2014, **43**, 9860–9871, DOI: **10.1039/C4DT00349G**.

15 A. K. Ambast, J. Goutam, S. Som and S. K. Sharma, $Ca_{1-x-y}Dy_xK_yWO_4$: A novel near UV converting phosphor for white light emitting diode, *Spectrochim. Acta, Part A*, 2014, **122**, 93–99, DOI: **10.1016/J.SAA.2013.11.032**.

16 S. H. Park, K. H. Lee, S. Unithrattil, H. S. Yoon, H. G. Jang and W. Bin Im, Melilite-structure $CaYAl_3O_7:Eu^{3+}$ phosphor: Structural and optical characteristics for near-UV LED-based white light, *J. Phys. Chem. C*, 2012, **116**, 26850–26856, DOI: **10.1021/JP307192Y/ASSET/IMAGES/LARGE/JP-2012-07192Y_0010.JPEG**.

17 D. Navami, R. B. Basavaraj, S. C. Sharma, B. Daruka Prasad and H. Nagabhushana, Rapid identification of latent fingerprints, security ink and WLED applications of $CaZrO_3:Eu^{3+}$ fluorescent labelling agent fabricated via bio-template assisted combustion route, *J. Alloys Compd.*, 2018, **762**, 763–779, DOI: **10.1016/J.JALLCOM.2018.05.016**.

18 P. Sehrawat, A. Khatkar, P. Boora, M. Kumar, R. K. Malik, S. P. Khatkar and V. B. Taxak, Emanating cool white light emission from novel down-converted $SrLaAlO_4:Dy^{3+}$ nanophosphors for advanced optoelectronic applications, *Ceram. Int.*, 2020, **46**, 16274–16284, DOI: **10.1016/J.CERAMINT.2020.03.184**.

19 N. Hussain, S. Rubab and V. Kumar, Spectroscopic characterizations and investigation of Judd-Ofelt intensity parameters of Dy^{3+}-doped $Ba_2La_8(SiO_4)_6O_2$ near white light emitting phosphor, *Ceram. Int.*, 2023, **49**, 15341–15348, DOI: **10.1016/j.ceramint.2023.01.118**.

20 F. Li, L. Li, C. Guo, T. Li, H. Mi Noh and J. H. Jeong, Up-conversion luminescence properties of Yb^{3+}-Ho^{3+} co-doped $CaLa_2ZnO_5$, *Ceram. Int.*, 2014, **40**, 7363–7366, DOI: **10.1016/j.ceramint.2013.12.080**.

21 Q. Ning, C. Zhou and Y. Shi, Effect of Eu^{3+} doping on $ZnWO_4$ phosphors luminescent properties and study of J-O theory, *J. Solid State Chem.*, 2020, **290**, 121458, DOI: **10.1016/J.JSSC.2020.121458**.

© 2023 The Author(s). Published by the Royal Society of Chemistry

Open Access Article. Published on 03 2023. Downloaded on 2025/5/31 23:29:15.
This article is licensed under a Creative Commons Attribution-NonCommercial 3.0 Unported Licence.

22 A. H. Wako, F. B. Dejene and H. C. Swart, Combustion synthesis, characterization and luminescence properties of barium aluminate phosphor, *J. Rare Earths*, 2014, **32**, 806–811, DOI: 10.1016/S1002-0721(14)60145-9.

23 P. M. Maleka, L. Reddy, T. J. Nkosi, A. Balakrishna, R. E. Kroon, H. C. Swart and O. M. Ntwaeaborwa, Structural and morphological characterization of photoluminescent cerium-doped near UV-blue sodium ortho-phosphate phosphors, *J. Lumin.*, 2020, **226**, 117409, DOI: 10.1016/J.JLUMIN.2020.117409.

24 A. Balakrishna, L. Reddy, O. M. Ntwaeaborwa and H. C. Swart, Remarkable influence of alkaline earth ions on the enhancement of fluorescence from Eu^{3+} ion doped in sodium ortho-phosphate phosphors, *J. Mol. Struct.*, 2020, **1203**, 127375, DOI: 10.1016/J.MOLSTRUC.2019.127375.

25 S. S. Pitale, M. Gohain, I. M. Nagpure, O. M. Ntwaeaborwa, B. C. B. Bezuidenhoudt and H. C. Swart, A comparative study on structural, morphological and luminescence characteristics of $Zn_3(VO_4)_2$ phosphor prepared via hydrothermal and citrate-gel combustion routes, *Phys. B*, 2012, **407**, 1485–1488, DOI: 10.1016/J.PHYSB.2011.09.067.

26 A. K. Kunti, L. Ghosh, S. K. Sharma and H. C. Swart, Synthesis and luminescence mechanism of white light emitting Eu^{3+} doped $CaZnV_2O_7$ phosphors, *J. Lumin.*, 2019, **214**, 116530, DOI: 10.1016/J.JLUMIN.2019.116530.

27 L. Li, C. Guo, S. Jiang, D. K. Agrawal and T. Li, Green up-conversion luminescence of Yb^{3+}-Er^{3+} co-doped $CaLa_2ZnO_5$ for optically temperature sensing, *RSC Adv.*, 2014, **4**, 6391–6396, DOI: 10.1039/c3ra47264g.

28 H. R. Shih, Y. Y. Tsai, K. T. Liu, Y. Z. Liao and Y. S. Chang, The luminescent properties of Pr^{3+} ion-doped BaY_2ZnO_5 phosphor under blue light irradiation, *Opt. Mater.*, 2013, **35**, 2654–2657, DOI: 10.1016/j.optmat.2013.08.007.

29 V. Singh, P. Halappa, N. Singh, M. S. Pathak, C. Shivakumara and V. Natarajan, EPR and Optical Properties of UV-B Radiation-Emitting Gd^{3+} -Doped $BaLa_2ZnO_5$ Host Prepared by Sol–Gel Method, *J. Electron. Mater.*, 2019, **48**, 3415–3422, DOI: 10.1007/S11664-019-07122-9/METRICS.

30 P. Sehrawat, R. K. Malik, M. Sheoran and R. Punia, Generation of cost-effective conventional-combustion derived novel green-luminous $BaLa_2ZnO_5$:Er^{3+} nanomaterials for high quality illumination in WLEDs and solar-cells, *Chem. Phys. Lett.*, 2021, **777**, 138752, DOI: 10.1016/j.cplett.2021.138752.

31 J. Song, X. Zhang, N. Huang, H. Dou, B. Chen, X. Tian, C. Wang and L. Wu, Luminescence properties and thermometric performance of Bi^{3+}/Sm^{3+}-codoped $BaLa_2ZnO_5$ phosphors, *Ceram. Int.*, 2023, **49**, 15229–15236, DOI: 10.1016/j.ceramint.2023.01.105.

32 P. Sehrawat, R. K. Malik, R. Punia, S. Maken and N. Kumari, Ecofriendly synthesis and white light-emitting properties of $BaLa_2ZnO_5$:Dy^{3+} nanomaterials for lighting application in NUV-WLEDs and solar cells, *Chem. Phys. Lett.*, 2022, **792**, 139399, DOI: 10.1016/J.CPLETT.2022.139399.

33 V. Singh, G. Lakshminarayana and A. Wagh, Photoluminescence Investigation on Green-Emitting Tb^{3+}-Doped $BaLa_2ZnO_5$ Nanophosphors, *J. Electron. Mater.*, 2020, **49**, 510–517, DOI: 10.1007/s11664-019-07734-1.

34 V. Singh, G. Lakshminarayana, D. E. Lee, J. Yoon and T. Park, Luminescence properties of reddish orange emitting $BaLa_2ZnO_5$:Sm^{3+} phosphor prepared by citric based sol-gel synthesis, *Solid State Sci.*, 2019, **98**, 106042, DOI: 10.1016/J.SOLIDSTATESCIENCES.2019.106042.

35 H. Dahiya, M. Dalal, J. Dalal, V. B. Taxak, S. P. Khatkar and D. Kumar, Synthesis and luminescent properties of Tb^{3+} doped $BaLa_2ZnO_5$ nanoparticles, *Mater. Res. Bull.*, 2018, **99**, 86–92, DOI: 10.1016/j.materresbull.2017.11.005.

36 J. Xie, L. Mei, L. Liao, M. Guan and H. Liu, Synthesis and up-conversion luminescence properties of Ho^{3+}, Yb^{3+} co-doped $BaLa_2ZnO_5$, *J. Phys. Chem. Solids*, 2015, **83**, 152–156, DOI: 10.1016/J.JPCS.2015.04.006.

37 S. Gai, H. Zhu, P. Gao, C. Zhou, Z. Kong, M. S. Molokeev, Z. Qi, Z. Zhou and M. Xia, Structure analysis, tuning photoluminescence and enhancing thermal stability on Mn^{4+}-doped $La_{2-x}Y_xMgTiO_6$ red phosphor for agricultural lighting, *Ceram. Int.*, 2020, **46**, 20173–20182, DOI: 10.1016/j.ceramint.2020.05.095.

38 P. Sehrawat, A. Khatkar, S. Devi, A. Hooda, S. Singh, R. K. Malik, S. P. Khatkar and V. B. Taxak, An effective emission of characteristic cool white light from Dy^{3+} doped perovskite type $SrLa_2Al_2O_7$ nanophosphors in single-phase pc WLEDs, *Chem. Phys. Lett.*, 2019, **737**, 136842, DOI: 10.1016/j.cplett.2019.136842.

39 P. Sehrawat, R. K. Malik, S. P. Khatkar and V. B. Taxak, Highly efficient green-glimmering $Y_3Al_5O_{12}$:Er^{3+} NPs for next generation electro-optic appliances, mainly white-LEDs and solar-cells, *Chem. Phys. Lett.*, 2021, **773**, 138592, DOI: 10.1016/J.CPLETT.2021.138592.

40 P. Sehrawat, R. K. Malik, R. Punia, M. Sheoran, S. Singh and M. Kumar, New Ba_2YAlO_5:Dy^{3+} nanomaterials for WLEDs: Propellant combustion synthesis and photometric features for enhanced emission of cool-white light under NUV excitation, *Chem. Phys. Lett.*, 2021, **781**, 138985, DOI: 10.1016/j.cplett.2021.138985.

41 P. Sehrawat, S. P. Khatkar, I. Jin Kim, R. K. Malik, P. Chhillar and V. B. Taxak, Realization of tricolor luminescence from novel $Sr_5Al_2O_8$:Sm^{3+}, Er^{3+}& Dy^{3+} nanomaterials for advanced photonic applications, *Chem. Phys. Lett.*, 2021, **762**, 138134, DOI: 10.1016/J.CPLETT.2020.138134.

42 P. Sehrawat, R. K. Malik, R. Punia, M. Sheoran, N. Kumari, S. P. Khatkar and V. B. Taxak, Luminescence tuning and structural analysis of new $BaYAlZn_3O_7$:Sm^{3+} nanomaterials with excellent performance for advanced optoelectronic appliances, *J. Mater. Sci.: Mater. Electron.*, 2021, **32**, 15930–15943, DOI: 10.1007/s10854-021-06144-6.

43 T. Samanta, A. E. Praveen and V. Mahalingam, Host sensitized intense infrared emissions from Ln^{3+} doped $GdVO_4$ nanocrystals: ranging from 950 nm to 2000 nm, *J. Mater. Chem. C*, 2018, **6**, 4878–4886, DOI: 10.1039/C8TC00841H.

44 G. Blasse, Energy transfer between inequivalent Eu^{2+} ions, *J. Solid State Chem.*, 1986, **62**, 207–211, DOI: 10.1016/0022-4596(86)90233-1.

© 2023 The Author(s). Published by the Royal Society of Chemistry

Open Access Article. Published on 03 2023. Downloaded on 2025/5/31 23:29:15.
This article is licensed under a Creative Commons Attribution-NonCommercial 3.0 Unported Licence.

45 J. Zhao, H. Gao, H. Xu, Z. Zhao, H. Bu, X. Cao, L. He, Z. Yang and J. Sun, Structure and photoluminescence of Eu^{3+} doped Sr_2InTaO_6 red phosphor with high color purity, *RSC Adv.*, 2021, **11**, 8282–8289, DOI: **10.1039/D1RA00165E**.

46 Q. Meng, B. Chen, W. Xu, Y. Yang, X. Zhao, W. Di, S. Lu, X. Wang, J. Sun, L. Cheng, T. Yu and Y. Peng, Size-dependent excitation spectra and energy transfer in Tb^{3+}-doped Y_2O_3 nanocrystalline, *J. Appl. Phys.*, 2007, **102**, 093505, DOI: **10.1063/1.2803502**.

47 Y. Tian, B. Chen, B. Tian, R. Hua, J. Sun, L. Cheng, H. Zhong, X. Li, J. Zhang, Y. Zheng, T. Yu, L. Huang and Q. Meng, Concentration-dependent luminescence and energy transfer of flower-like $Y_2(MoO_4)_3$:Dy^{3+} phosphor, *J. Alloys Compd.*, 2011, **509**, 6096–6101, DOI: **10.1016/J.JALLCOM.2011.03.034**.

48 H. Shihua and L. Liren, Concentration dependence of sensitizer fluorescence intensity in energy transfer, *Chin. J. Lumin.*, 1990, **11**, 1–7.

49 S. Dutta, S. Som and S. K. Sharma, Luminescence and photometric characterization of K+ compensated $CaMoO_4$:Dy^{3+} nanophosphors, *Dalton Trans.*, 2013, **42**, 9654–9661, DOI: **10.1039/C3DT50780G**.

50 B. R. Judd, Optical absorption intensities of rare-earth ions, *Phys. Rev.*, 1962, **127**, 750–761, DOI: **10.1103/PhysRev.127.750**.

51 G. S. Opelt, Intensities of Crystal Spectra of Rare-Earth Ions, *J. Chem. Phys.*, 2004, **37**, 511, DOI: **10.1063/1.1701366**.

52 S. Dutta, S. Som and S. K. Sharma, Excitation spectra and luminescence decay analysis of K+ compensated Dy^{3+} doped $CaMoO_4$ phosphors, *RSC Adv.*, 2015, **5**, 7380–7387, DOI: **10.1039/C4RA12447B**.

53 W. Luo, J. Liao, R. Li and X. Chen, Determination of Judd–Ofelt intensity parameters from the excitation spectra for rare-earth doped luminescent materials, *Phys. Chem. Chem. Phys.*, 2010, **12**, 3276–3282, DOI: **10.1039/B921581F**.

54 M. L. Meena, C. H. Lu, S. Som, R. Chaurasiya and S. D. Lin, Highly efficient and thermally stable Eu^{3+} activated phosphate based phosphors for wLEDs: An experimental and DFT study, *J. Alloys Compd.*, 2022, **895**, 162670, DOI: **10.1016/j.jallcom.2021.162670**.

55 S. Dutta, S. Som, M. L. Meena, R. Chaurasiya and T. M. Chen, Multisite-Occupancy-Driven Intense Narrow-Band Blue Emission from $Sr_5SiO_4C_{l6}$:Eu^{2+} Phosphor with Excellent Stability and Color Performance, *Inorg. Chem.*, 2020, **59**, 1928–1939, DOI: **10.1021/ACS.INORGCHEM.9B03222/SUPPL_FILE/IC9B03222_SI_001.PDF**.

56 H. Zhou, Y. Jin, M. Jiang, Q. Wang and X. Jiang, A single-phased tunable emission phosphor $MgY_2Si_3O_{10}$:Eu^{3+},Bi^{3+} with efficient energy transfer for white LEDs, *Dalton Trans.*, 2014, **44**, 1102–1109, DOI: **10.1039/C4DT02114B**.

57 S. Tanabe, J. Kang, T. Hanada and N. Soga, Yellow/blue luminescences of Dy^{3+}-doped borate glasses and their anomalous temperature variations, *J. Non-Cryst. Solids*, 1998, **239**, 170–175, DOI: **10.1016/S0022-3093(98)00734-0**.

© 2023 The Author(s). Published by the Royal Society of Chemistry